

# Radiative forcing from aircraft NO<sub>x</sub> emissions: mechanisms and seasonal dependence

David Stevenson<sup>†</sup>, Ruth Doherty<sup>†</sup>, Mike Sanderson<sup>‡</sup>, Bill Collins<sup>‡</sup>, Colin Johnson<sup>‡</sup>, and Dick Derwent<sup>†</sup>

<sup>†</sup>Institute of Atmospheric and Environmental Science, The University of Edinburgh, EH9 3JZ, UK

<sup>‡</sup>Hadley Centre for Climate Prediction and Research, The Met. Office, UK

<sup>†</sup>rdscientific, Newbury, Berkshire, UK

David.S.Stevenson@ed.ac.uk



## 0 Quick summary:

- Ø Add a month-long pulse of aircraft NO<sub>x</sub> to CTM – follow for 5 years
- Ø Impacts of the pulse cascade through the model's chemistry
- Ø Analyse in detail how the pulse perturbs global O<sub>3</sub> and OH budgets
- ΔOH is mainly controlled by ΔNO<sub>x</sub> and ΔO<sub>3</sub>, not ΔCO
- NO<sub>x</sub> pulse generates short-lived O<sub>3</sub> increase and long-lived CH<sub>4</sub> decrease
- Emissions pulses in different months show some seasonal variations
- Calculate time-integrated O<sub>3</sub> and CH<sub>4</sub> radiative forcings
- Net global radiative forcing from aircraft NO<sub>x</sub> is approximately zero

**1** We performed 5 experiments with the STOCHEM CTM: a 5-yr control, then 4 repeat runs with 10x aircraft NO<sub>x</sub> emissions in January, April, July and October of the 1st year. **Figure 1** shows perturbations to the global burdens of NO<sub>x</sub>, O<sub>3</sub>, OH and CH<sub>4</sub> for the 4 pulse experiments, relative to the control. The different months had slightly different magnitude emission pulses; results were linearly scaled to 1 Tg(NO<sub>x</sub>) pulses in all the figures, to make them directly comparable. The NO<sub>x</sub> and OH anomalies are very short-lived, reflecting the rapid turnover times of these species in the atmosphere. The extra NO<sub>x</sub> generates O<sub>3</sub> for a few months after the pulse. The extra OH<sub>4</sub> enhances the CH<sub>4</sub> destruction flux, depleting CH<sub>4</sub> for a few months. The CH<sub>4</sub> anomaly then starts to decay with an e-folding time of 11.1 yr (the CH<sub>4</sub> perturbation lifetime<sup>1</sup>; 39% longer than the CH<sub>4</sub> lifetime). This long-lived CH<sub>4</sub> depletion has an associated small negative O<sub>3</sub> anomaly. Most aircraft emissions are in the Northern Hemisphere; hence the July pulse experiences mainly summer conditions, with shorter residence times for NO<sub>x</sub> and O<sub>3</sub>, more OH production, and consequently a larger CH<sub>4</sub> depletion.

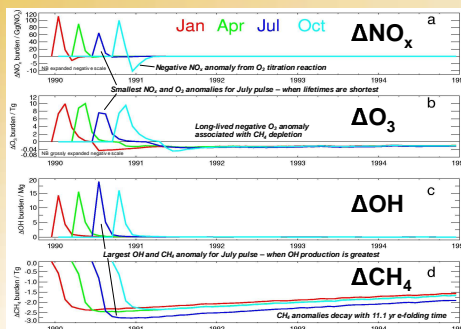


**Figure 1** Model global burdens relative to control run

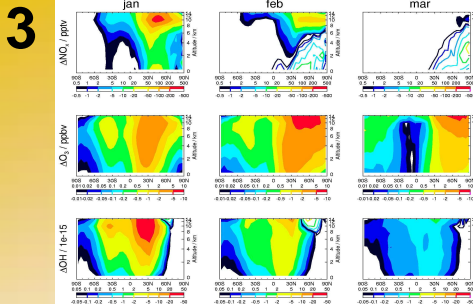


**Figure 3** Zonal mean perturbations to NO<sub>x</sub>, O<sub>3</sub> and OH for three months during/after the January pulse.

**4** To understand the mechanisms responsible for the OH anomaly, it is useful to look at the spatial and temporal structure of the main perturbations to the OH budget in more detail (**Figure 4**). This figure shows monthly zonal mean plots of the main perturbations to OH production and loss fluxes, for the same three months as **Figure 3**, and for the main reactions in **Figure 2**. The first three rows of **Figure 4** display perturbations to OH production fluxes (reactions 1-3), whilst the last two rows show perturbations to OH loss fluxes (reactions 4 and 5). The loss fluxes are multiplied by minus one, so that all positive values (filled contours) in **Figure 4** represent enhanced OH sources, whereas all negative values (open contours) show enhanced OH sinks. Reaction 1 (1<sup>st</sup> row of **Figure 4**) mainly reflects changes in NO<sub>x</sub> (1<sup>st</sup> row of **Figure 3**). Reactions 2 and 3 (2<sup>nd</sup> and 3<sup>rd</sup> rows of **Figure 4**) are largely controlled by the extra O<sub>3</sub> (2<sup>nd</sup> row of **Figure 3**), although reaction 3 is also affected by changes in HO<sub>2</sub> via reaction 1 in the UT/LS. The CH<sub>4</sub> oxidation flux perturbation distribution is very important, as this illustrates where the methane loss occurs – predominantly in the mid-troposphere at 10-30°N during the first month, and at 0-30°N in the lower troposphere subsequently. The source of the OH driving the enhanced CH<sub>4</sub> oxidation comes from a combination of reactions 1 and 2 initially, then from reactions 2 and 3. This illustrates that the source of OH arising through the O<sub>3</sub> route is important in determining the CH<sub>4</sub> perturbation, as O<sub>3</sub> transport and mixing represents a mechanism for transporting the aircraft impact from the mid-latitude UT to the tropical lower troposphere. Similar behaviour is seen for the aircraft pulses in other seasons. Isaksen et al.<sup>2</sup> suggested that CO could play an important role in spreading the aircraft impact, but we find that perturbations to CO oxidation (reaction 4) act mainly to reduce OH, and thus cannot contribute to the enhanced CH<sub>4</sub> oxidation. Only in the 3<sup>rd</sup> (and subsequent) months (**Figure 2**) does the perturbation to CO oxidation become an OH source, but by this time most of the CH<sub>4</sub> anomaly has already been generated.

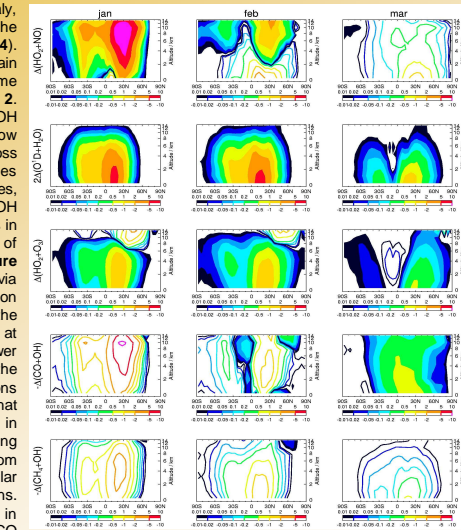


**Figure 4** Zonal mean perturbations to the main OH production (top 3 rows) and loss (bottom 2 rows) fluxes (ppbv/month) for 3 months during/after the January pulse. Loss fluxes are multiplied by -1: hence filled contours represent extra OH sources; open contours extra OH sinks.

**2** **Figure 2** shows the impact of the January pulse on the global OH budget. The main initial source of extra OH is reaction **R1**. This source rapidly declines following the pulse, due to the short NO<sub>x</sub> lifetime, eventually becoming an OH sink as the NO<sub>x</sub> anomaly turns negative (**Fig. 1a**). By the 2<sup>nd</sup> month, the dominant extra OH source is **R2**, which is driven upwards by the rise in O<sub>3</sub>. The only other significant OH source term (**R3**) is also related to O<sub>3</sub>. The two most important OH sink reactions that rise in response to elevated OH are **R4** and **R5**. Two months after the pulse, the main extra OH source term is due to a reduced flux through the sink **R4**, driven by the reduction in CO built up over the first two months. The enhanced CH<sub>4</sub> oxidation flux (**R5**) results in a global depletion of CH<sub>4</sub> (**Fig. 1d**), that accumulates over the first 5-6 months, mainly occurring in the first 2 months. The reduction of CH<sub>4</sub> also causes **R5** to switch over to become an OH source after 6 months, through a similar mechanism to **R4**. **R4** responds more quickly because of CO's shorter lifetime. These OH budget perturbations have important spatial distributions, which are explored next.

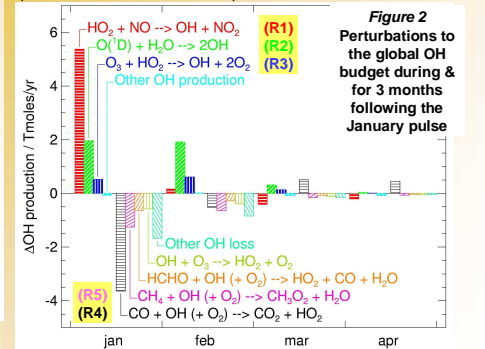


**Figure 2** Perturbations to the global OH budget during & for 3 months following the January pulse

**5** To estimate the overall climate forcing from aircraft NO<sub>x</sub> emissions, time-integrated radiative forcings were calculated for the O<sub>3</sub> and CH<sub>4</sub> perturbations, over a 100-yr time horizon [e.g. Wild et al.<sup>3</sup>]. For CH<sub>4</sub>, because the perturbation is long-lived it becomes well-mixed throughout the atmosphere, so the radiative forcing calculation is relatively straightforward. The July pulse yields the most negative time-integrated CH<sub>4</sub> radiative forcing (**Figure 5**). For O<sub>3</sub>, the perturbation has two stages (**Figure 1b**): a short-lived (~6 months) positive phase (with a distinct spatial structure: **Figure 3**), followed by a long-lived (and hence more geographically homogeneous) negative phase, associated with (and decaying at the same rate as) the negative CH<sub>4</sub> anomaly. Because the numerical experiments were only 5 years long, the anomalies were extrapolated out to 100-yr using the 11.1 yr e-folding timescale. Ozone anomalies have been converted to radiative forcings using an off-line radiation code, taking full account of stratospheric temperature adjustment, which reduces instantaneous forcings by ~22%. The initial positive forcing is largest for the April emissions pulse, and least for the January pulse (**Figure 5**). This represents a complex trade-off between net O<sub>3</sub> production chemistry (highest in April), O<sub>3</sub> lifetime (longest in January), and forcing per O<sub>3</sub> molecule (highest in July). The integrated long-term O<sub>3</sub> forcing is 17-20% of the short-term positive forcing. We find net forcings close to zero.

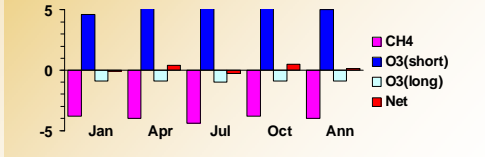


**Figure 5** Time-integrated radiative forcings (mW m<sup>-2</sup> yr)

**6** These results have a number of important caveats. The size of the pulse may influence the results, as O<sub>3</sub> and OH photochemistry responds in a strongly non-linear fashion to NO<sub>x</sub>. The transport, mixing (including convection) and chemistry schemes in the model will influence the results, and these are still quite variable between different models and remain poorly constrained. Nevertheless, similar results from an independent study<sup>3</sup> are encouraging.

**Acknowledgements**  
We thank the Environment Agency (P4-F02), Natural Environment Research Council (NER/J/S/2000/00840, NER/T/S/2000/01041), and the Government Meteorological Research programme (DEFRA contract CPEA7) for funding.

**References**  
<sup>1</sup>Prather, M et al., Atmospheric Chemistry and Greenhouse Gases, In: *Climate Change 2001: The Scientific Basis*, Contribution of WG1 to the Third Assessment report of the IPCC, Eds. JT Houghton et al., Cambridge University Press, UK, 2001.  
<sup>2</sup>Isaksen, ISA et al., Modelling the chemical composition of the future atmosphere, In: *IPCC Special report on Aviation and the global atmosphere*, eds. JE Penner et al., pp. 121-163, Cambridge University Press, UK, 1999.  
<sup>3</sup>Wild, O, MJ Prather, and H Akimoto, Indirect long-term global radiative cooling from NO<sub>x</sub> emissions, *Geophys. Res. Lett.*, 28(9), 1719-1722, 2001.